ISSN 0016-7932, Geomagnetism and Aeronomy, 2016, Vol. 56, No. 6, pp. 761–773. © Pleiades Publishing, Ltd., 2016.
Original Russian Text © V.M. Sorokin, A.K. Yashchenko, 2016, published in Geomagnetizm i Aeronomiya, 2016, Vol. 56, No. 6, pp. 800–813.

# Anomalous Propagation of VHF Radiowaves behind the Horizon in the Seismic Region

**V. M. Sorokin* and A. K. Yashchenko**

*Pushkov Institute of Terrestrial Magnetism, Ionosphere, and Radiowave Propagation (IZMIRAN), Russian Academy of Sciences, Troitsk, Moscow, 142190 Russia*

**e-mail: sova@izmiran.ru*

Received November 16, 2015; in final form, February 20, 2016

**Abstract**—A theory of electromagnetic radiation generation by random electric discharges in the troposphere and VHF radiowave scattering by these discharges has been developed. The discharge model, which makes it possible to calculate the spatiotemporal distribution of the discharge channel conductivity depending on the electric current value in this discharge, has been obtained. The electromagnetic radiation spectrum in the troposphere occupied by random discharges has been calculated. VHF electromagnetic wave scattering by random electric discharges in the troposphere has been considered. Equations have been derived, and the method for calculating the average value of the electromagnetic wave field scattered by random discharges has been developed. The calculations indicated that the scattered wave field amplitude is much larger than the diffraction wave field amplitude behind the horizon. The theoretical results agree with the observations of the electromagnetic radiation and VHF transmitter signals behind the horizon relative to the earthquake epicenter during the earthquake preparation.

**DOI:** 10.1134/S0016793216050133

## 1. INTRODUCTION

Many electromagnetic phenomena related to seismic activity are known at different frequencies (Varotsos and Alexopoulos, 1984; Gokhberg et al., 1995; Nagao et al., 2002; Hayakawa, 2009). Two types of anomalies exist: anomalies of emissions and electromagnetic signal propagation. These phenomena occupy a wide spectral region of electromagnetic disturbances from quasi-static fields to high frequencies. We present some results of observations of anomalous phenomena. Using a radar, Voinov et al. (1992) detected that distributed charges appeared in the atmosphere above the Spitak earthquake epicenter one to three days before its onset. The regions of distributed charges differed from similar regions originating during thunderstorms in the time characteristics and location height. The timescale of variations in discharged regions was several hours, whereas this scale is not longer than an hour for thunderstorm activity (Proctor et al., 1988). The height and horizontal dimension of charged regions were also unusual. Their height was 5–30 km, and the area was larger than a similar area related to thunderstorms by almost an order of magnitude (Warwick et al., 1979). Hata et al. (1998) detected the electromagnetic radiation at a frequency of 225 Hz, which is generated in the atmosphere near the sea surface during seismic activity in the zone of underwater faults. The emission source was localized based on the measurements of the emission magnetic components (Hata et al., 1996). Before a powerful earthquake ($M = 7.3$) in China, a nightglow was observed at a distance of up to 100–200 km from the earthquake epicenter (Zhao and Qian, 1997). In the review of optical phenomena related to earthquakes in the Mediterranean Sea region (Papadopoulos, 1999), it is emphasized that the optical effects are observed above land and sea, as a rule, for earthquakes with magnitudes larger than 6.0. It is also reported (Williams et al., 1989) that the maximal distance to the epicenter was 140 km. For these cases, the luminosity altitude can reach several kilometers. VHF radio emissions originating before earthquakes were for the first time regularly observed during several years on Crete since 1992. The observations were performed with two receivers at frequencies of 41 and 53 MHz located at four stations (Nomikos et al., 1997; Vallianatos and Nomikos, 1998). The VHF radioemission was registered before earthquakes, the epicenters of which were located on land and below the sea bottom. Based on the obtained data, it was shown (Ruzhin and Nomicos, 2006) that the VHF emission source was in the troposphere at altitudes about several kilometers above the earthquake preparation epicenter.

The main results are as follows.

—A signal was registered for many earthquakes when continuous observations were performed during three years.

—A signal was repeatedly registered at two VHFs (41 and 53 MHz) and at several stations simultaneously.

—VHF radiation sources were located behind the horizon at distances of 300–350 km from receivers.

—A signal was observed during several days before an earthquake in the daytime and at night.

—The center of marine earthquakes was below the sea bottom, and the radiation source was in the atmosphere above the surface of this center.

Yamada et al. (2002) confirmed the conclusion that VHF radiaition sources are localized in the atmosphere at an altitude of several kilometers. As a result of prolonged observations performed from July 1999 at Tatayama staton (Chiba prefecture), the earthquake-related VHF emission (52.1–52.5 MHz) was detected. The direction toward earthquake epicenters was within the receiving antenna pattern. Since the diatance to the epicenters was several hundred kilometers, they can be registered only if their source was at a height of several kilometers in the atmosphere.

These observations presented in (Fukumoto et al., 2001; Moriya et al., 2010) indicated that the VHF signals of transmitters, the propagation paths of which extend over the earthquake preparation epicentral region, are considerably amplified when seismic activity increases. The earthquake preparation near the VHF radiowave propagation path from Sendai City broadcasting station to Tateyama observatory was accompanied by anomalous earthquake characteristics (Sakai et al., 2001). Using the observational data behind the horizon, Fukumoto et al. (2001) confirmed that cases of anomalous propagation resulted from VHF radiowave scattering immediately before an earthquake. Using directional antennas in order to receive signals, Pilipenko et al. (2001) indicated that VHF radiowaves are scattered in the middle atmosphere.

The phenomena considered above were interpreted in (Sorokin et al., 2011, 2012a, 2012b, 2014). It was shown that thin (about several kilometers) layers with a horizontal dimension about a hundred of kilometers, where the quasi-static electric field approaches breakdown values, can originate at altitudes of 5–10 km above the earthquake epicenter during its preparation. The train of statistically independent electric discharges can be generated in this altitudinal region as a result of atmospheric turbulence. The breakdown field value depends on the atmospheric density; therefore, the density fluctuation in a turbulent vortex results in an electric discharge in the case when the external electric field value is close to its breakdown value. Similar electric discharges are observed before a lightning discharge in thunderclouds. They were called "preliminary breakdown pulse trains" (Rakov and Uman, 2003). The electric field generation during an earthquake preparation is considered in detail in (Sorokin and Hayakawa, 2013; Sorokin et al., 2015). Electric discharges in the troposphere above the epicentral zone generate electromagnetic noise in the VHF range, which is observed behind the horizon relative to the impending earthquake source. They result in an anomalous propagation of VHF transmitter radiowaves as a result of radiowave scattering by random discharges, which are located in the tropospheric region near the propagation path. As a result, the wave amplitude behind the horizon considerably increases as compared to the transmitter wave that propagates behind the horizon as a result of diffraction.

Below, we develop the electric discharge model that makes it possible to calculate the spatiotemporal conductivity distribution depending on the current value in a discharge. Based on this model, we considered the emission of random discharges and radiowave scattering by these discharges.

## 2. MODEL OF ELECTRIC DISCHARGE IN THE ATMOSPHERE

The processes proceeding in a discharge can be represented in the form of two stages. A pulse current, which generates the electromagnetic radiation in a wide frequency range, flows in the initial discharge stage. Certain temperature and electric conductivity distributions are subsequently formed in a discharge channel. These distributions are the initial conditions when the second process stage is modeled. During the next stage, a channel cools, and its electric conductivity decreases. An incident monochromatic electromagnetic wave emitted by an extraneous source is effectively scattered during this stage. To model the first discharge stage, we should select the spatiotemporal dependence of the discharge current and calculate the temperature and conductivity distributions that were formed after termination of the current flow. For the second discharge stage, we should model discharge channel cooling and the relaxation of its conductivity dependent on the channel temperature. Subsequently, it is necessary to calculate the current induced by an incident monochromatic wave in the conducting channel with a specified nonstationary conductivity. During the first discharge stage, the emission is caused by a pulse current with a duration of $\sim 10^{-7}$ s. Since a monochromatic wave is incident on a discharge, the emission is caused by a quasiharmonic current with a period of $10^{-7}$–$10^{-8}$ s during the second stage. The current amplitude damps during $10^{-3}$–$10^{-4}$ s. This model will be used to calculate the spatial distribution of the electromagnetic field strength generated by the set of statistically independent sources located in the troposphere.

We introduce the Cartesian coordinate system $(x, y, z)$ with axis $z$ directed vertically upward. A vertically oriented discharge with length $l$ is located along the $z$ axis in the interval $0 < z < l$. To determine the discharge current value ($I$), we will use the model

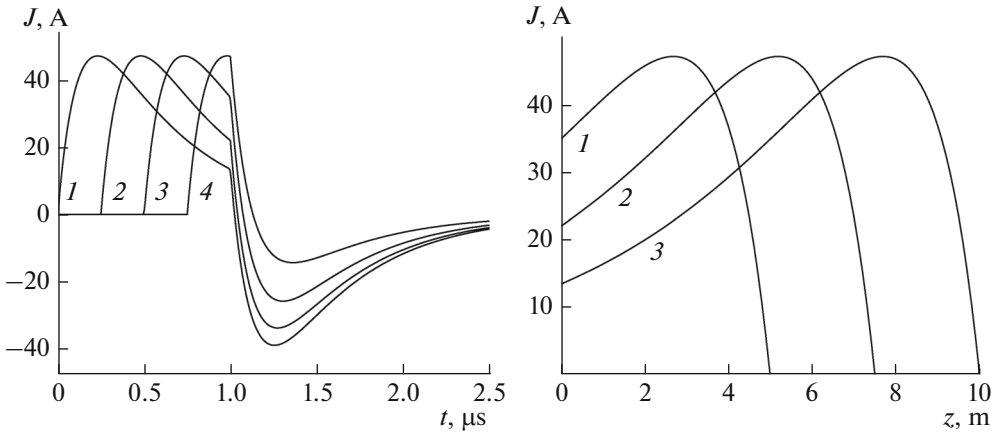


**Fig. 1.** Time variations in the discharge current (left panel) at (*1*) $z = 0$; (*2*) $z = l/4$; (*3*) $z = l/2$; and (*4*) $z = 3l/4$. The dependence of the discharge current on coordinate (right panel) at (*1*) $t = t/4$; (*2*) $t = t/2$; and (*3*) $t = t$.

accepted in (Iudin and Trakhtengerts, 2001; Sorokin et al., 2011):

$$I(z,t) = I_0\{\eta(t - z/u)[\exp(-\alpha(t - z/u)) - \exp(-\beta(t - z/u))] - \eta(t - \tau)[\exp(-\alpha(t - \tau)) - \exp(-\beta(t - \tau))]\}; \quad \tau = l/u, \tag{1}$$

where $\eta(t)$is the Heaviside function; $u$ is the current pulse propagation velocity along a discharge channel; $I_0 = 250$ A; $u = 2\times10^7$ m/s; $l = 10$ m; $\alpha,\beta$ are the parameters characterizing the duration of the current front and pulse decrease, $\alpha = 2/\tau$, $\beta = 8/\tau$ (Sorokin et al., 2012a). The dependence of the discharge current $I(z,t)$ on coordinates and time is shown in Fig. 1. The plots show that the current wave propagates from $z = 0$ to $z = l$ at velocity $u$, reflects once with the sign reversal at $z = l$, and then damps very rapidly.

To determine the characteristics of the discharge plasma channel, which was formed after the flow of a pulse current during the first discharge stage, we use the Toepler semiempirical law (Voldman, 2004), which relates the discharge channel running conductivity $G(z)$ to the current flowing in this channel:

$$G(z) = 2\pi\int_0^\infty \sigma_0(r,z)rdr = k_T\int_0^\infty |I(z,t)|dt; \quad k_T = 250\ \text{mV}^{-1}\ \text{s}^{-1}, \tag{2}$$

where $\sigma_0(r,z)$ is the initial radial distribution of the discharge conductivity after the current flow. The integration in relationship (2) is performed over the cross section of an axially symmetric channel. Function $G(z)$ is the integral characteristic of the plasma channel state in the initial stage of its cooling. Running conductivity $G(z)$ corresponds to a certain radial distribution of the temperature and electric conductivity, which depends on this temperature in the state of thermodynamic equilibrium. According to (Williams et al., 1989), the electron collision frequency with molecules is $\nu_{en} = 6\times10^9$ s$^{-1}$ when the discharge plasma temperature is $T = 5000$. Since the characteristic circular frequency of the considered electromagnetic waves ($\omega \sim 10^8$ s$^{-1}$) is much lower than the characteristic collision frequency of electrons with molecules $\nu_{en}$, we can assume that the discharge channel conductivity is stationary. Figure 2 presents dependence $G(z)$. The plot indicates that the running conductivity varies within 0–0.015 m ohm$^{-1}$. We introduced the average discharge channel conductivity using the formula

$$G_0 = \frac{1}{l}\int_0^l G(z)dz. \tag{3}$$

The heated air conductivity is calculated in (Yos, 1963). The calculations indicate that conductivity $\sigma(T)$ can be approximated by the following formula at 2000–10000 K

$$\sigma(T) = \sigma_m \exp(-T_m/T); \quad \sigma_m = 1.62\times10^5\ \text{Cm/m};\ \ T_m = 4\times10^4\ \text{K}. \tag{4}$$

Assume that the radial distribution of the discharge channel temperature, which is formed after the current flow, is defined by the Gauss function in the cylindrical coordinate system $(r,\varphi,z)$

$$T(r,0) = T_e + (T_0 - T_e) \times \exp(-r^2/r_0^2) \approx T_0\exp(-r^2/r_0^2), \quad T_e = 300\ \text{K} \ll T_0, \tag{5}$$

where $T_e$ is the ambient temperature and $T_0$ is the temperature on the discharge channel axis. Substituting

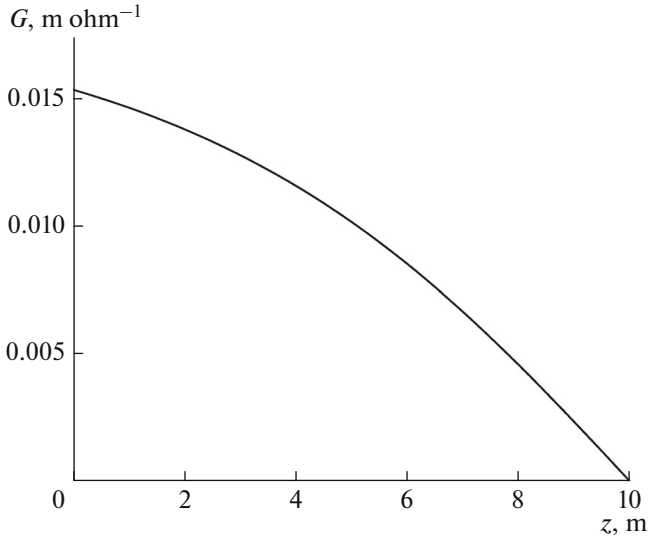


**Fig. 2.** Dependence of discharge channel running conductivity $G(z)$ on coordinate.

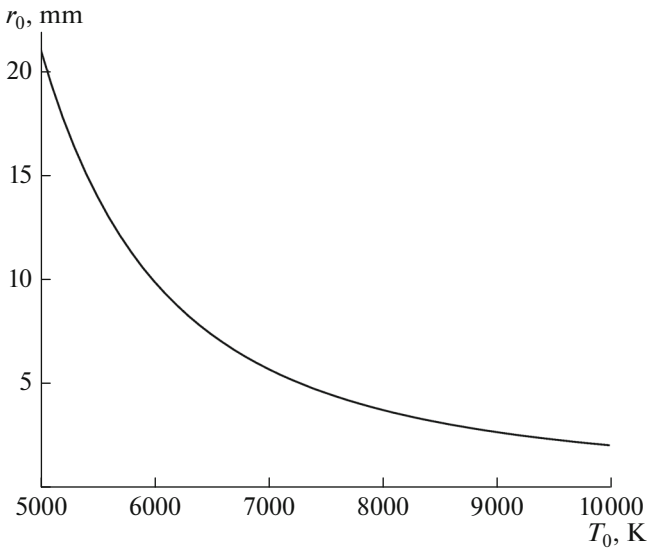


**Fig. 3.** Dependence of discharge channel thermal radius $r_0$ on initial temperature $T_0$ on its axis.

expression (5) in (2), we obtain the equation connecting quantities $G_0$, $T_0$, and $r_0$:

$$G_0 = 2\pi\sigma_m \int_0^\infty \exp\left[-\frac{T_m}{T_0}\exp\left(r^2/r_0^2\right)\right] r dr. \qquad (6)$$

The value of running conductivity $G_0$ is determined from equalities (3) and (2). Expression (6) characterizes the relationship between parameters $T_0$, $r_0$ of the discharge temperature spatial distribution (5). Inequality $T_m/T_0 \gg 1$ makes it possible to determine explicitly the discharge channel thermal radius ($r_0$) as a function of temperature $T_0$ on its axis:

$$r_0 \approx \sqrt{\frac{G_0}{\pi\sigma_m}\frac{T_m}{T_0}}\exp\left(\frac{T_m}{2T_0}\right). \qquad (7)$$

The estimates indicate that the running conductivity value for the discharge current parameters selected above is $G_0 = 5\times10^{-3}$ m ohm$^{-1}$. According to (Orville, 1967), the characteristic temperature of discharges with linear dimensions ~10 m is not more than $T_0 \le 10^4$ K. Figure 3 presents dependence $r_0(T_0)$, which is calculated with formula (7). The plot indicates that the discharge characteristic thermal radius is $2\times10^{-3}$–$1.5\times10^{-2}$ m at $T_0 \le 10^4$. The specific $r_0$ value can be selected based on the condition of the best fit of the electromagnetic disturbance calculations to the observational data.

We now consider cooling of a longitudinally homogeneous and axially symmetric discharge channel, where the initial temperature distribution is specified by formulas (4) and (7). This process depends on the effects of diffusive and convective energy transport and is modeled with the axially symmetric equations of thermal conductivity, continuity, motion, and state.

We will use the following approximation, which was proposed in (Uman and Voshall, 1968), in order to calculate the dynamics of a lightning discharge cooling channel: the pressure in the channel is constant and is equal to the atmospheric pressure. Consequently, the air density is a single-valued function of temperature: $\rho = \rho(T)$. We can show that, using this approximation, as well as the equation of state and the temperature dependences for specific heat capacity $c_p(T)$ and air thermal conductivity κin the considered temperature range $5\times10^3$–$10^4$ K (Creagh et al., 1963; Yos, 1963)

$$\rho(T) = \frac{a}{T^2};\quad c_p(T) = bT;\quad a = 1.5\times10^6\ \frac{\mathrm{K}^2\ \mathrm{kg}}{\mathrm{m}^3};$$
$$b = 1\ \frac{\mathrm{J}}{\mathrm{K}^2\ \mathrm{kg}};\quad \kappa \approx \overline{\kappa} = 1\ \frac{\mathrm{J}}{\mathrm{K\ kg}}, \qquad (8)$$

we can reduce the calculation of the discharge axisymmetric channel cooling dynamics to the solution the following equation defining a dimensionless temperature:

$$\frac{\partial f}{\partial\tau} = -2\left(\frac{\partial f}{\partial\xi}\right)^2 + \frac{f}{\xi}\frac{\partial f}{\partial\xi} + f\frac{\partial^2 f}{\partial\xi^2};$$
$$f(\xi,\tau) = T/T_0;\quad \xi = \frac{r}{r_0};\quad \tau = \frac{t}{t_0};\quad t_0 = \frac{r_0^2}{kT_0}, \qquad (9)$$

with the following initial and boundary conditions

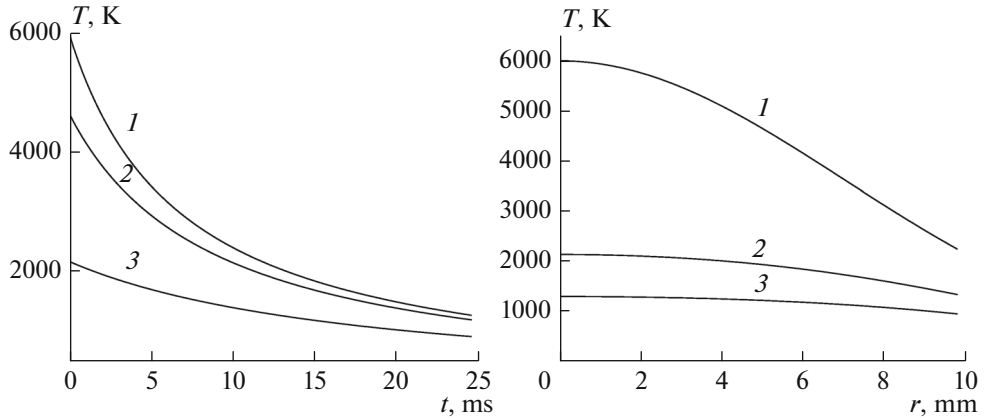


**Fig. 4.** Time variations in the discharge channel temperature (left panel) at different distances from the axis: (*1*) $r = 0$; (*2*) $r = r_0/2$; (*3*) $r = r_0$. The dependence of the discharge channel temperature on radius (right panel) at different instants: (*1*) $t = 0$; (*2*) $t = t_0/2$; (*3*) $t = t_0$.

$$f(\xi,0) = \exp\left(-\xi^2\right);\ \left.\frac{\partial f}{\partial \xi}\right|_{\xi=0} = 0;\ \ f\big|_{\xi\to\infty} = 0, \quad (10)$$

where $k = \kappa/ab = 6.6\times10^{-7}$ m$^2$ s$^{-1}$ K$^{-1}$. An analysis of the numerical solution of system (9), (10) indicated that this solution can be approximated by the following formula with a satisfactory accuracy

$$f(\xi,\tau) = \frac{\exp\left(-\xi^2\right)}{1+\alpha\exp\left(-\xi^2\right)\tau}. \quad (11)$$

According to the calculations, a minimum of the rms deviation of formula (11) from the numerical solution is reached when $\alpha = 3.6$, and the conductivity approximation is the best at $\alpha \approx 4$. The characteristic time of conducting channel cooling at $r_0 = 10^{-2}$ m; $T_0 = 8000$ K is $t_0 = 20$ ms.

Figure 4 presents the time and spatial dependences of the discharge channel temperature. The following parameter values were selected for the calculation: $G_0 = 0.012$ m ohm$^{-1}$; $T_0 = 6000$ K; $r_0 = 10$ mm; $t_0 = 25$ ms.

The plots indicate that the characteristic thermal radius of a discharge channel reaches 10 mm, and the channel lifetime is several milliseconds. The cooling characteristic time increases with increasing distance from the channel axis, and the characteristic channel radius increases on long timescales. Substituting (11) in (4), we obtain the approximate formula for the spatial–time dependence of conductivity in the form:

$$\sigma(r,t) = \sigma_1\exp\left(-\frac{r^2+r_0^2}{r_1^2}-\frac{t}{t_1}\right);$$
$$r_1 = r_0\sqrt{T_0/T_m};\ \ t_1 = t_0T_0/\alpha T_m. \quad (12)$$

Consequently, the time variation in the discharge channel conductivity is a damped exponential curve. A similar dependence was used in (Sorokin et al., 2014) in order to calculate the wave field scattered by discharges. The characteristic relaxation time ($t_1$) is scaled proportionally to the channel thermal radius squared $r_0$. The radial temperature distribution is approximately Gaussian, and its spatial scale is a factor of $\sqrt{T_0/T_m}$ as small as the temperature scale $r_0$. Figure 5 presents the discharge conductivity variations depending on the discharge time, temperature, and radius for $r_1 = 4$ mm; $t_1 = 1$ ms.

The plots indicate that the characteristic relaxation time of the discharge channel conductivity is ~1 ms, and the channel characteristic radius is 1–2 mm.

## 3. INDUCED CURRENT IN A DISCHARGE CONDUCTING CHANNEL

The electric field of a wave scattered by a conducting discharge is generated by a current induced in an incident wave discharge. We will assume that a linearly polarized monochromatic wave is incident on a vertically oriented discharge and has the electric field vertical component (**E**) defined by the expression

$$E(t) = E_0\cos(\omega_0 t) = \mathrm{Re}\left[E_0\exp(-i\omega_0 t)\right],$$

where $E_0, \omega_0$ are the incident wave amplitude and frequency, respectively. A discharge with length $l$ is a conductor with an axially symmetric distribution of conductivity $\sigma(r,t)$, which depends on time. The spatiotemporal distribution of the discharge channel conductivity is defined by formula (12). We calculate the current induced in a discharge in an approximation of long transmission lines (Sadiku, 2007). We verified the validity of using a long transmission line approximation in the calculations by comparing the data

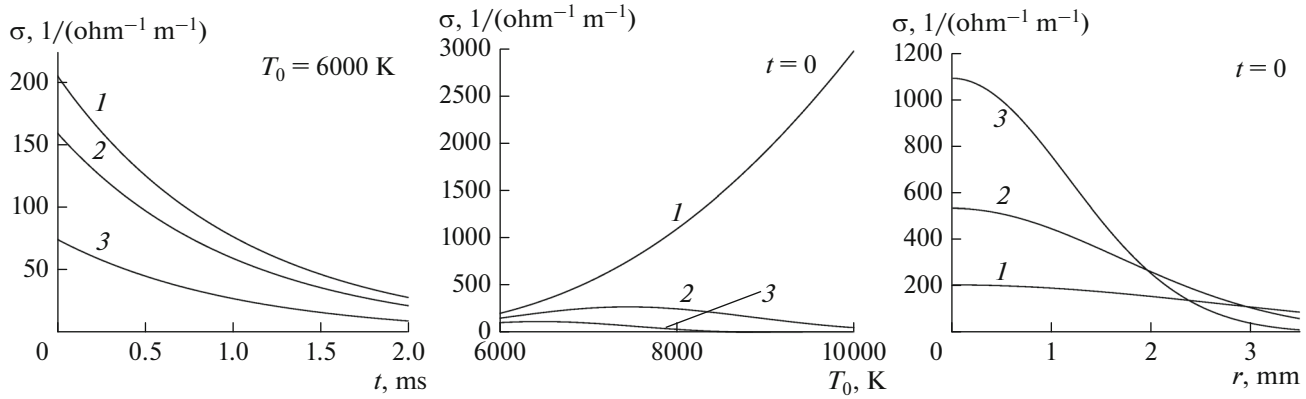


**Fig. 5.** Time variations in the discharge channel conductivity (left panel) at different distances from the axis: (*1*) $r = 0$; (*2*) $r = r_1/2$; (*3*) $r = r_1$. The dependence of the discharge channel conductivity on temperature (middle panel) at different distances from the axis: (*1*) $r = 0$; (*2*) $r = r_1/2$; (*3*) $r = r_1$. The dependence of the discharge channel conductivity on radius (right panel) for different discharge initial temperature: (*1*) $T_0 = 6000$ K; (*2*) $T_0 = 7000$ K; (*3*) $T_0 = 8000$ K.

obtained using this approximation and by solving numerically the problem of scattering a monochromatic electromagnetic wave by a thin long imperfect conductor using the Pocklington integral equation. These calculations indicated that an approximation of long transmission lines can be applied rather accurately in the considered range of the problem parameters. In this approximation the discharge-conducting channel is a cylindrical conductor. We write $a$ for the cylinder radius. This radius is an effective conductor radius, which is determined from the condition of equality of the conductivity current absolute value and the bias current in a conductor where conductivity depends on radius:

$$\sigma(a) = \varepsilon_0\omega_0. \tag{13}$$

Thus, a discharge-conducting channel with a radial conductivity distribution is replaced by a cylindrical conductor with an effective radius, with only a conductivity current within this conductor and only a bias current outside it. Neglecting the relatively weak dependence of the effective radius on time, from expressions (7), (12), and (13), we obtain

$$\begin{aligned} a &\approx r_1\sqrt{\ln\left(\frac{\sigma_m}{\varepsilon_0\omega_0}\right) - \frac{T_m}{T_0}} \\ &= \sqrt{\frac{G_0}{\pi\sigma_m}}\exp\left(\frac{T_m}{2T_0}\right)\sqrt{\ln\left(\frac{\sigma_m}{\varepsilon_0\omega_0}\right) - \frac{T_m}{T_0}}. \end{aligned} \tag{14}$$

We estimate the effective radius value ($a$). Selecting the values of the discharge temperature and incident wave frequency $T_0 = 8\times10^3$ K; $\omega_0 = 5\times10^8$ s$^{-1}$, we find that $a = 1.58r_0$. This value indicated that the conductor effective radius is larger than the characteristic scale of the discharge temperature radial distribution.

In an approximation of long lines, the conductor surface potential ($V$) and the electric current flowing along a conductor ($I$) are defined by the equations:

$$\begin{aligned} &-\frac{\partial V}{\partial z} - L\frac{\partial I}{\partial t} = RI + E_0\cos(\omega_0 t); \quad C\frac{\partial V}{\partial t} + \frac{\partial I}{\partial z} = 0; \\ &C = \frac{2\pi\varepsilon_0}{\log(l/a)}; \quad L = \frac{\mu_0}{2\pi}\log(l/a) = \varepsilon_0\mu_0/C = c^2/C, \end{aligned} \tag{15}$$

where $L,C$ are the induction and capacity of a conductor unit length, respectively, $\varepsilon_0$ is the electric constant, $\mu_0$ is magnetic permittivity of vacuum, and $c$ is the velocity of light. We place the origin at the conductor center. The current vanishes at conductor edges:

$$I(\pm l/2, t) = 0. \tag{16}$$

Resistance $R$ per conductor unit length is defined as a ratio of the electric field longitudinal component on the conductor surface to current $I$:

$$R = \frac{E(a)}{I} = \frac{E(a)}{2\pi\int\limits_0^a \sigma(r,t)\,E(r)\,r\,dr}. \tag{17}$$

To calculate conductor resistivity $R(\omega_0, t)$, we use the Maxwell quasistationary equations characterizing the radial distribution of components $E, H_\varphi$ of the electric and magnetic fields within a conductor. Neglecting the bias current and relatively small longitudinal components, we obtain:

$$\frac{dE}{dr} = -i\omega\mu_0 H_\varphi; \quad \frac{1}{r}\frac{d}{dr}(rH_\varphi) = \sigma E. \tag{18}$$

From relationships (17) and (18) we have

$$R = \frac{E(a)}{2\pi a H_\varphi(a)}. \tag{19}$$

We determine conductor impedance $Z(a) = E(a)/H_\varphi(a)$ and admittance $Y(a) = 1/Z(a)$. Consequently, the relationship for conductivity (19) can be expressed in terms of these quantities:

$$R = \frac{Z(a)}{2\pi a} = \frac{1}{2\pi a Y(a)}. \quad (20)$$

We introduce dimensionless admittance $g$ and radius $x$ using the formulas

$$g(x,t) = Y(x,t)/r_1\sigma_0(t); \quad x = r/r_1;$$
$$\sigma_0(t) = \sigma_m \exp(-T_m/T_0 - t/t_1).$$

Using formula (12), from Eqs. (18), we can obtain the Riccati differential equation defining function $g$:

$$\frac{dg}{dx} = \exp(-x^2) - \frac{g}{x} + ikg^2; \quad g(0) = 0;$$
$$0 \le x \le x_m; \quad x_m = a/r_1; \quad k(t) = \mu_0\omega_0\sigma_0(t)r_1^2. \quad (21)$$

Solving Eqs. (21) numerically for different values of dimensionless parameter $k(t)$, we obtain the function of two variables $g(x, k(t))$, which will make it possible to determine resistivity $R$ using formula (20):

$$R(\omega_0,t) = 1/2\pi r_1^2 x_m \sigma_0(t)\, g(x_m, k(t)). \quad (22)$$

Figure 6 presents the time variations in discharge channel resistivity $R(\omega_0,t)$ as a result of channel cooling, which is calculated with formulas (21) and (22) for the incident electromagnetic wave frequency ($f_0 = \omega_0/2\pi = 80$ MHz). The calculations indicate that the resistivity growth rate increases with increasing discharge initial temperature. The characteristic value of this rate is ~100 ohm m$^{-1}$.

Taking into account that discharge channel conductivity $\sigma$ slowly changes as compared to incident wave period $2\pi/\omega_0$, we can represent the current induced by a wave in a charge and the current potential in the form:

$$I(z,t) = \mathrm{Re}[I_0(z,t)\exp(-i\omega_0 t)],$$
$$V(z,t) = \mathrm{Re}[V_0(z,t)\exp(-i\omega_0 t)], \quad (23)$$

where $I_0, V_0$ are the wave functions slowly varying in time as compared to period $2\pi/\omega_0$. Substituting (23) in (15) and eliminating $V_0(z,t)$, we obtain the equation for determining function $I_0$:

$$\frac{d^2 I_0}{dz^2} + q^2(t) I_0 = i\omega_0 C E_0.$$

The solution of this equation with boundary condition (16) has the form:

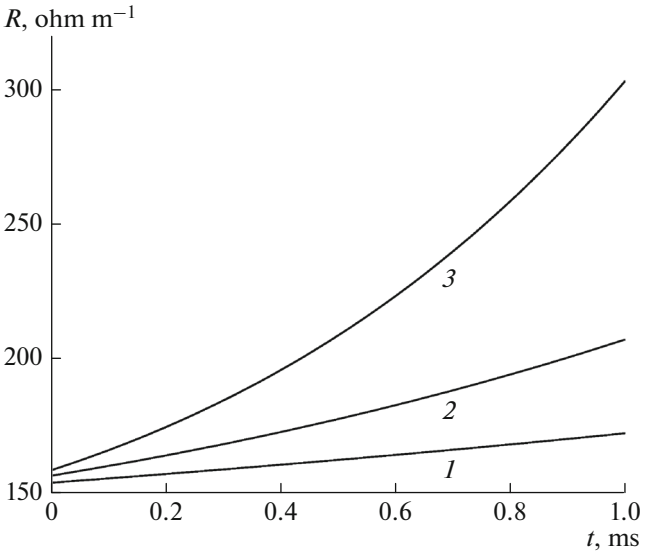


**Fig. 6.** Time variations in discharge channel resistivity $R(\omega_0,t)$ for different values of the channel initial temperature: (*1*) $T_0 = 5000$ K; (*2*) $T_0 = 5500$ K; (*3*) $T_0 = 6000$ K.

$$I(z,t) = \mathrm{Re}[I_0(z,t)\exp(-i\omega_0 t)];$$
$$I_0(z,t) = \frac{i\omega_0 C l^2 E_0}{[q(t)l]^2}\left\{1 - \frac{\cos[q(t)z]}{\cos[q(t)(l/2)]}\right\}; \quad (24)$$
$$q^2(t) = (\omega_0/c)^2 + i\omega_0 C R(\omega_0,t),$$

where $R(\omega_0,t)$ is defined by formula (22). Equality (24) makes it possible to calculate the current value in a discharge induced by an incident monochromatic electromagnetic wave.

## 3. ELECTROMAGNETIC RADIATION GENERATED BY STATISTICALLY INDEPENDENT SOURCES

We consider the electromagnetic radiation generated by discharges that originate at random points and in a certain tropospheric area, where the strength of a quasi-static electric field approaches the breakdown value. We represent this area as a set of fixed cells and attach index $k$ to these cells. The characteristic cell dimension is about the discharge spatial scale. Each discharge occurs in one of the cells, and the discharge instants in each cell form the sequence of random values $t_{k\alpha} = t_{k1}, t_{k2}, \ldots$. We introduce the Cartesian coordinate system with axis $z$ directed vertically upward and the origin located on the Earth's surface. We denote the spatio-temporal distribution of the current density in each discharge by $\mathbf{j}_{k\alpha}^{(+)} = \mathbf{j}_{k\alpha}\left(\mathbf{r} - \mathbf{r}_k^{(+)}, t - t_{k\alpha}\right)$, where $\mathbf{r}_k^{(+)} = (x_k, y_k, z_k)$ is the discharge center radius vector. In the initial stage, the intrinsic radiation is caused by the discharge current. The electromagnetic

wave scattered by a discharge is caused by the charge current induced by an incident wave. Assuming that the Earth's surface is a perfectly conducting plane, we denote the discharge current representation in this plane by $\mathbf{j}_{k\alpha}^{(-)} = \mathbf{j}_{k\alpha}\left(\mathbf{r} - \mathbf{r}_k^{(-)},\ t - t_{k\alpha}\right)$, where $\mathbf{r}_k^{(-)} = (x_k, y_k, -z_k)$ is the representation radius vector. The schematic location and representations of a discharge current are presented in (Sorokin et al., 2014).

The strengths of the electric $\mathbf{E}_{k\alpha}$ and magnetic $\mathbf{H}_{k\alpha}$ fields of the discharge emission and its representations are defined by the Maxwell equations:

$$\nabla \times \mathbf{H}_{k\alpha} = \mathbf{j}_{k\alpha}^{(+)} + \mathbf{j}_{k\alpha}^{(-)} + \varepsilon_0 \frac{\partial \mathbf{E}_{k\alpha}}{\partial t};$$

$$\nabla \times \mathbf{E}_{k\alpha} = -\mu_0 \frac{\partial \mathbf{H}_{k\alpha}}{\partial t},$$

$$\nabla \cdot \mathbf{E}_{k\alpha} = \frac{\rho_{k\alpha}^{(+)} + \rho_{k\alpha}^{(-)}}{\varepsilon_0};\quad \nabla \cdot \mathbf{H}_{k\alpha} = 0,$$

where $\rho_{k\alpha}^{(\pm)}$ is the charge density in a discharge and its representation. The field of the electromagnetic radiation of the region occupied by discharges is defined by the equalities:

$$\mathbf{E} = \sum_{k\alpha} \mathbf{E}_{k\alpha};\quad \mathbf{H} = \sum_{k\alpha} \mathbf{H}_{k\alpha}. \tag{25}$$

We consider the field on the Earth's surface. In this case the observation point radius vector ($\mathbf{r}$) is located in plane $(x, y)$. In the Fraunhofer zone $\left|\mathbf{r} - \mathbf{r}_k^{(+)}\right| \gg l^2/\lambda$ (where $\lambda$ is the characteristic emission wavelength), the discharge emission field and vector potentials $\mathbf{A}_{k\alpha}^{(\pm)}(\mathbf{r}, t)$ are defined by the approximate formulas (Van Bladel, 2007):

$$\mathbf{E}_{k\alpha} = \sum_{\mu=\pm}\left(\frac{\partial \mathbf{A}_{k\alpha}^{(\mu)}}{\partial t} \times \mathbf{n}_k^{(\mu)}\right) \times \mathbf{n}_k^{(\mu)};\quad \mathbf{H}_{k\alpha} = \frac{1}{Z_0}$$

$$\times \sum_{\mu=\pm}\left(\frac{\partial \mathbf{A}_{k\alpha}^{(\mu)}}{\partial t} \times \mathbf{n}_k^{(\mu)}\right);\quad \mathbf{A}_{k\alpha}^{(\pm)}(\mathbf{r}, t) = \frac{\mu_0}{4\pi\left|\mathbf{r} - \mathbf{r}_k^{(\pm)}\right|} \tag{26}$$

$$\times \int \mathbf{j}_{k\alpha}\left(\mathbf{r}', t - t_{k\alpha} - \frac{\left|\mathbf{r} - \mathbf{r}_k^{(\pm)}\right|}{c} + \frac{\mathbf{n}_k^{(\pm)} \cdot \mathbf{r}'}{c}\right) \mathrm{d}\,\mathbf{r}';$$

$$Z_0 = \sqrt{\mu_0/\varepsilon_0};\quad \mathbf{n}_k^{(\pm)} = \left(\mathbf{r} - \mathbf{r}_k^{(\pm)}\right)\Big/\left|\mathbf{r} - \mathbf{r}_k^{(\pm)}\right|.$$

A Fraunhofer approximation for a discharge with a length of $l \sim 10$ m and $\lambda \sim 3$ m is satisfied when distances from a source to an observation point are $\left|\mathbf{r} - \mathbf{r}_k\right| \sim 30$ m. The integration is performed over an emitting current volume. Since the discharge current flows in a thin vertically oriented conducting channel with length $l$, the vertical component of the current density vector ($j_{k\alpha}$) can be represented in the form

$$j_{k\alpha} = I(x_k, y_k, z - z_k, t - t_{k\alpha})\delta(x - x_k)\delta(y - y_k), \tag{27}$$

where $I$ is the spatio-temporal current distribution in a discharge channel, and $\delta(x)$ is the Dirac delta function.

On the surface of a perfectly conducting Earth, the electric field tangential component vanishes, and the vertical component and the magnetic field strength double. Substituting (27) and (26) in (25), we obtain the formulas for the electric and magnetic field components on the Earth's surface:

$$E_z(\mathbf{r}, t) = -\frac{\mu_0}{2\pi}\sum_{k,\alpha}\frac{1 - n_{kz}^2}{\left|\mathbf{r} - \mathbf{r}_k\right|}\frac{\partial}{\partial t}\int_{-l/2}^{l/2} d\xi$$

$$\times I\left(\mathbf{r}_k, \xi, t - t_{k\alpha} - \frac{\left|\mathbf{r} - \mathbf{r}_k\right|}{c} + \frac{n_{kz}\xi}{c}\right);$$

$$\mathbf{H}_\perp(\mathbf{r}, t) = \frac{\mu_0}{2\pi Z_0}\sum_{k,\alpha}\frac{(\mathbf{e}_z \times \mathbf{n}_{k\perp})}{\left|\mathbf{r} - \mathbf{r}_k\right|}\frac{\partial}{\partial t}\int_{-l/2}^{l/2} d\xi \tag{28}$$

$$\times I\left(\mathbf{r}_k, \xi, t - t_{k\alpha} - \frac{\left|\mathbf{r} - \mathbf{r}_k\right|}{c} + \frac{n_{kz}\xi}{c}\right),$$

where $\mathbf{r}_k^{(+)} \to \mathbf{r}_k$. In formulas (28) the integration is performed over the discharge conducting channel length $z - z_k = \xi$. Electromagnetic field (28) is the total emission of cells generated by their currents. These expressions indicate, for example, that the vertical component of the electric field can be written in the following general form:

$$E_z(\mathbf{r}, t) = \sum_{k,\alpha} f_k(t - t_{k\alpha});\quad f_k(t) = -\frac{\mu_0}{2\pi}\frac{\left(1 - n_{kz}^2\right)}{\left|\mathbf{r} - \mathbf{r}_k\right|}$$

$$\times \frac{\partial}{\partial t}\int_{-l/2}^{l/2} d\xi I\left(\mathbf{r}_k, \xi, t - \frac{\left|\mathbf{r} - \mathbf{r}_k\right|}{c} + \frac{n_{kz}\xi}{c}\right). \tag{29}$$

The magnetic field horizontal components have a similar form. Therefore, we consider below the electric field component. To determine such statistical characteristics of a random process as the mean value and the correlation function, we assume that instants $t_{k\alpha} = \{t_{k1}, t_{k2} \ldots\}$ form Poisson sequences with frequencies $\nu_k$ for each cell with number $k$ (Yaglom, 1987). Assuming that random quantities that belong to cells with different numbers $k$ are statistically independent, from (29) we obtain:

$$\left\langle E_z(\mathbf{r}, t)\right\rangle = \sum_k \nu_k \int_{-\infty}^{\infty} f_k(t)\, dt = 0;\quad P_z^{(E)}(\mathbf{r}, t)$$

$$= \left\langle E_z(\mathbf{r}, t + \tau) E_z(\mathbf{r}, \tau)\right\rangle \tag{30}$$

$$= \sum_k \nu_k \int_{-\infty}^{\infty} f_k(\tau + t)\, f_k(\tau)\, d\tau.$$

The first formula in system (30) follows from the fact that function $f_k(t)$ is the time derivative of the finite function. The power spectrum of the electric

field vertical component $\tilde{P}_z^{(E)}(\mathbf{r},\omega)$ is defined as a Fourier transform of correlation function $P_z^{(E)}(\mathbf{r},t)$:

$$\tilde{P}_z^{(E)}(\mathbf{r},\omega) = \int_{-\infty}^{\infty} dt \exp(i\omega t) P_z^{(E)}(\mathbf{r},t) = \sum_k \nu_k \left|\tilde{f}_k(\mathbf{r},\mathbf{r}_k,\omega)\right|^2. \quad (31)$$

In equality (31) we identify:

$$\tilde{f}_k(\omega) = \frac{i\omega\mu_0}{2\pi}\frac{1-n_{kz}^2}{|\mathbf{r}-\mathbf{r}_k|}\exp\left(i\omega\frac{|\mathbf{r}-\mathbf{r}_k|}{c}\right) \times \int_{-l/2}^{l/2} d\xi \tilde{I}(\mathbf{r}_k,\xi,\omega)\exp\left(-i\omega\frac{n_{kz}\xi}{c}\right);$$

$$\tilde{I}(\mathbf{r}_k,\xi,\omega) = \int_{-\infty}^{\infty} dt\ \exp(i\omega t)\ I(\mathbf{r}_k,\xi,t).$$

We determine the discharge frequency volumetric density $N(\mathbf{r}_k)$ in a cell with number $k$ using the $\nu_k = N(\mathbf{r}_k)\Delta V_k$ formula, where $\Delta V_k$ is the $k$th cell volume. Replacing the summation over $k$ in (31) by the integration over volume $V$ of the region occupied by discharges, according to formula $\sum_k \nu_k F(\mathbf{r}_k) = \int_V N(\mathbf{r}')F(\mathbf{r}')d\mathbf{r}'$, we obtain

$$P_z^{(E)}(\mathbf{r},\omega) = \left(\frac{\omega\mu_0}{2\pi}\right)^2 \times \int_V N(\mathbf{r}')\frac{\left(1-n_z^2\right)^2}{|\mathbf{r}-\mathbf{r}'|^2}\left|\tilde{D}(\mathbf{r},\mathbf{r}',\omega)\right|^2 \mathrm{d}\,\mathbf{r}'. \quad (32)$$

We find the power spectrum of the horizontal components of the emission magnetic field in a similar manner

$$P_{x,y}^{(H)}(\mathbf{r},\omega) = \left(\frac{\omega\mu_0}{2\pi Z_0}\right)^2 \times \int_V N(\mathbf{r}')\frac{n_{y,x}^2}{|\mathbf{r}-\mathbf{r}'|^2}\left|\tilde{D}(\mathbf{r},\mathbf{r}',\omega)\right|^2 \mathrm{d}\,\mathbf{r}'. \quad (33)$$

In formulas (30) and (31), we identify:

$$\tilde{D}(\mathbf{r},\mathbf{r}',\omega) = \int_{-l/2}^{l/2} d\xi \tilde{I}(\mathbf{r},\xi,\omega)\exp\left(-i\omega\frac{n_z\xi}{c}\right); \quad \mathbf{n} = \frac{\mathbf{r}-\mathbf{r}'}{|\mathbf{r}-\mathbf{r}'|}. \quad (34)$$

In a point source approximation, which is valid at $l \ll \lambda$, the $\tilde{D}$ value is the Fourier transform of the current dipole moment:

$$D(\mathbf{r},t) = \int_{-l/2}^{l/2} I(\mathbf{r},\xi,t)d\xi. \quad (35)$$

Below we present the calculation of the emission electric field. The emission magnetic field components are calculated in a similar manner. For a broadband intrinsic radiation, the spatial distribution of the electric field vertical component $E_{zs}(\mathbf{r},\omega)$ at frequency $\omega$ is defined by the expression

$$E_{zs}(\mathbf{r},\omega) = \sqrt{\frac{1}{2\pi}P_{zs}^{(E)}(\mathbf{r},\omega)\Delta\omega}, \quad (36)$$

where the bandwidth ($\Delta\omega$) depends on the measuring equipment parameters. In formula (36) the $P_{zs}^{(E)}(\mathbf{r},\omega)$ value means power spectrum (32) of the intrinsic radiation of random discharges generated by current (1) that flows during the discharge initial stage. We determine the spatial distribution of the average value of the wave field vertical component $E_{zr}(\mathbf{r})$, which is scattered by random discharges, by integrating the power spectrum over frequency:

$$E_{zr}(\mathbf{r}) = \sqrt{\frac{1}{2\pi}\int_{-\infty}^{\infty} P_{zr}^{(E)}(\mathbf{r},\omega)\,d\omega}. \quad (37)$$

In formula (37) the $P_{zr}^{(E)}(\mathbf{r},\omega)$ value means power spectrum (32) scattered by random discharges of the emission generated by current (24) induced by an incident wave in a discharge. Formulas (32), (36), and (37) make it possible to calculate the spectral and spatial characteristics of the electric component of the random discharge intrinsic radiation and the emission scattered by these discharges at a random spatial distribution of the discharge frequency volumetric density. The characteristics of the emission magnetic component are calculated similarly.

To illustrate the achieved results, we calculate below the electric field of the intrinsic and scattered radiation for the generation of random discharges over a seismic region. We indicated (Sorokin et al., 2012b) that the characteristic vertical scale of the discharge generation region ($d_0$) in the troposphere is ~1 km, the horizontal scale is several ten kilometers, and the distance from this region center to the observation point is about several hundred kilometers. The discharge generation region is located at altitudes varying from 5 to 10 km. We approximate the discharge frequency spatial distribution $N(\mathbf{r})$ by a thin layer that is located at altitude $z_0$, using the expression

$$N(x,y,z) = 2N_m d_0\left(1-\frac{r^2}{r_0^2}\right)\eta\left(1-\frac{r^2}{r_0^2}\right)\delta(z-z_0), \quad (38)$$

where $N_m$ is the discharge frequency volumetric density at this region epicenter; $r_0$ is the radius of the discharge generation region; $\eta(z)$ is the unit function;

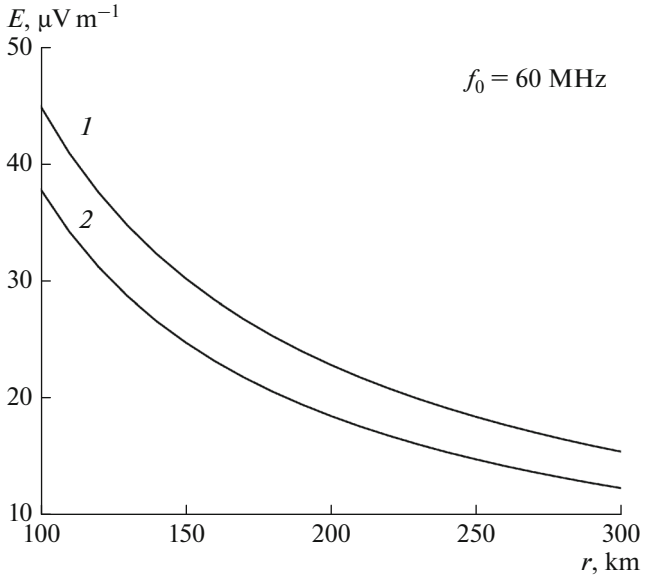


**Fig. 7.** Dependence of the amplitude of the electric field vertical component on distance: the intrinsic (*1*) and scattered (*2*) radiations.

$\delta(z)$ is the delta function. We will consider the emission field on the Earth's surface at large distances ($r$) as compared to the altitude ($h$) of the tropospheric layer including discharges, $n_z \sim h/r \ll 1$.

This means that we consider the electromagnetic radiation near the source equatorial plane.

The power spectrum of the discharge intrinsic radiation is defined by formula (52) obtained in Appendix. Substituting (52) in (36), we obtain:

$$E_{zs}(r,\omega) = \frac{1}{\sqrt{2\pi}}\frac{\omega\mu_0}{2\pi}|P(\omega)|\left|\tilde{\Phi}_s(\omega)\right|\sqrt{F(r)};$$
$$P(\omega) = \frac{I_0 u(\alpha-\beta)}{\omega\sqrt{\left(\alpha^2+\omega^2\right)\left(\beta^2+\omega^2\right)}}; \quad (39)$$
$$\Phi_s(\omega) = (1-i\omega\tau)\exp(i\omega\tau) - 1.$$

In equality (39) function $F(r)$ is defined by formula (51):

$$F(r) = 2\pi N_0 d_0\left[1+\left(\frac{r^2}{r_0^2}-1\right)\ln\left(1-\frac{r_0^2}{r^2}\right)\right]. \quad (40)$$

The power spectrum of the emission scattered by random discharges is defined by formula (52) obtained in Appendix. Substituting (40) in (37), we obtain:

$$E_{zr}(r) = \frac{1}{\sqrt{2\pi}}\frac{\omega\mu_0}{2\pi}P_0\left|\tilde{\Phi}_r(\omega-\omega_0)\right|\sqrt{F(r)};$$
$$P_0 = Cl^3E_m; \quad \tilde{\Phi}_r(\omega) = \int_{-\infty}^{\infty}\Phi_r(t)\exp(i\omega t)dt, \quad (41)$$

where $E_m = \sqrt{3Z_0W/2\pi\left(x_s^2+y_s^2\right)}$ is the value of the electric field of the transmitter incident wave in the region occupied by discharges, $(x_s, y_s)$ are the transmitter coordinates, $W$ is the transmitter power, and $Z_0 = \sqrt{\mu_0/\varepsilon_0} = 377$ ohm. In equality (41) we identify:

$$\Phi_r(t) = \frac{\omega_0}{(ql)^3}\left[\tan\left(\frac{ql}{2}\right)-\frac{ql}{2}\right];$$
$$q^2(t) = \left(\frac{\omega_0}{c}\right)^2 + i\omega_0 CR(\omega_0,t). \quad (42)$$

The discharge channel resistivity $R(\omega_0,t)$ is defined by formulas (21) and (22). At large distances $r \gg r_0$, from (40) we obtain asymptotics of function $F(r) \approx \pi N_0 d_0 r_0^2/r^2$. Consequently, the field amplitude decreases depending on distance as $1/r$. From (39) and (41) it follows that the signal spectra are factorized in both cases. In addition, if we neglect a relatively weak spatial dependence of the incident wave amplitude in the formula, $f \approx 1$, it is evident that the spatial dependences of the signal intensities of both considered types are identical. This is an important signature of the proposed model, which can be used for its experimental verification. Figures 7 and 8 present the spatial and frequency amplitude dependences of the observed electric fields of the intrinsic and scattered emissions. During the calculations, we selected the following values of the parameters (see (1), (5), and (38)) of the emission elementary source: $I_0 = 100$ A; $l = 10$ m; $u = 10^7$ m/s; $\alpha = 2u/l$, $\beta = 8u/l$; $T_0 = 5000$ K, the disturbed region: $r_0 = 50$ km; $d_0 = 0.5$ km; $z_0 = 6$ km; $N_m = 2.5\times10^{-5}$ $1/\text{m}^3$ s and the VHF transmitter: $x_s = -100$ km; $P = 5$ kW.

Figure 7 presents the intrinsic radiation amplitude at a frequency of $f_0 = 60$ MHz in a receiving equipment spectral window of $\Delta f = 20$ kHz and the scattered radiation amplitude of the VHF transmitter with carrier frequency $f_0$ depending on the epicentral distance. Figure 7 indicates that both values are of the same order of magnitude and vary from ~40 μV m$^{-1}$ at 100 km distance to ~10 μV m$^{-1}$ at 300 km distance. Such electric field values correspond in an order of magnitude to the observational results presented in (Nomikos et al., 1997; Vallianatos and Nomikos, 1998; Fukumoto et al., 2001; Moriya et al., 2010). Figure 8 presents the intrinsic radiation spectrum and the frequency dependence of the scattered radiation on the transmitter carrier frequency at a fixed epicentral distance of 300 km. Figure 8 indicates that the intrinsic radiation amplitude decreases with increasing frequency, and the scattered radiation amplitude increases with increasing transmitter carrier frequency. The amplitude values become equal at $f \approx 50$ MHz.

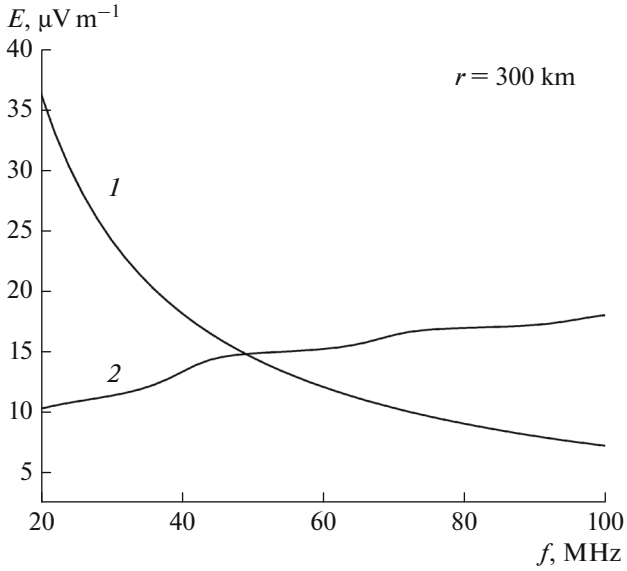


**Fig. 8.** Dependence of the amplitude of the electric field vertical component on frequency: the (*1*) intrinsic and scattered (*2*) radiations.

## 4. CONCLUSIONS

Continuous monitoring of the VHF electromagnetic emission for three years showed that the emission generation region is located in the atmosphere at altitudes of 1–10 km over the seismic region epicenter. The emission is observed for several days before the main earthquake shock. The registration of transmitter VHF signals behind the horizon showed that the signal amplitude substantially increases during the earthquake preparation if the earthquake epicenters are located near the signal propagation path. During the same period, a quasi-static electric field increases in the ionosphere to ~10 mV m$^{-1}$. The appearance of such a field in the ionosphere is related to the electric field that flows in the atmospheric–ionospheric circuit. The calculations indicated that the electric field of the conductivity current that flow between the atmosphere and ionosphere can reach the breakdown value in the troposphere at altitudes reaching 10 km. Atmospheric turbulence results in the formation of random electric discharges at these altitudes. These electric discharges cause the VHF emission. The VHF transmitter signals are scattered by discharges, since they have a considerable electric conductivity. The thickness of the region occupied by discharges is about several kilometers. The observed anomalous increase in the VHF transmitter signal amplitude behind the horizon is explained by the fact that an incident wave is scattered by discharges in the troposphere and propagates behind the horizon relative to a transmitter.

We developed here the electric discharge model, which makes it possible to find the spatio-temporal distribution of the discharge conductivity that originates as a result of air heating by the discharge current. We approximated the spatio-temporal dependence of the discharge current by a model pulse propagating along the discharge channel at a constant velocity. We used the semiempirical Toepler law in order to calculate the channel parameters after the termination of the current. Cooling of the discharge channel, which is responsible for the discharge conductivity relaxation dynamics, results from two processes: thermal conductivity and convection of a cooled gas toward the channel axis. The theory developed in the work makes it possible to calculate the random discharge electromagnetic emission spectrum at different distances and the spatio-temporal distribution of the average electric field of a wave scattered by these discharges. The performed calculations of the amplitude and frequency characteristics of the discharge emission showed that these calculations agree with the observational data. The calculations of the average transmitter field value behind the horizon are confirmed by the VHF signals observed in the seismic zone. The theory can be used to interpret the VHF signal characteristics related to thunderstorm activity.

## APPENDIX

We calculate the $\tilde{D}_s(\mathbf{r},\mathbf{r}',\omega)$ value using formula (34) in order to determine the spectrum of the random discharge intrinsic electromagnetic radiation, which is generated by the current in each discharge. Using the dependence of the discharge current on coordinates and time (1), we obtain from (34)

$$\tilde{D}_s(\mathbf{r},\mathbf{r}',\omega) = I_0 \frac{iu(\alpha-\beta)}{\omega(1-\gamma n_z)(\alpha-i\omega)(\beta-i\omega)} \times \left\{\exp(i\omega\tau)\left[1-\frac{1-\exp(-i\omega\gamma n_z\tau)}{\gamma n_z}\right]-1\right\}; \quad (43)$$
$$\gamma = u/c; \quad n_z = (z-z')/|\mathbf{r}-\mathbf{r}'|.$$

Substituting expression (43) in formula (32), we obtain the power spectrum of the electric field vertical component:

$$P_{zs}^{(E)}(\mathbf{r},\omega) = \left(\frac{\omega\mu_0}{2\pi}\right)^2 |P(\omega)|^2 \int_V N(\mathbf{r}') \frac{\left(1-n_z^2\right)^2}{|\mathbf{r}-\mathbf{r}'|^2} \times |\Phi_s(\omega,n_z)|^2 \, \mathrm{d}\mathbf{r}'; \quad P(\omega) = \frac{I_0 u(\alpha-\beta)}{\omega\sqrt{\left(\alpha^2+\omega^2\right)\left(\beta^2+\omega^2\right)}};$$
$$\Phi_s(\omega,n_z) = \frac{1}{1-\gamma n_z} \times \left\{\exp(i\omega\tau)\left[1-\frac{1-\exp(-i\omega\gamma n_z\tau)}{\gamma n_z}\right]-1\right\}.$$

Formula (32) indicates that the power spectrum depends on the spatial distribution of discharge frequency $N(\mathbf{r})$. Selecting this distribution in the form of

a thin layer (38) at large distances $n_z \sim h/r \ll 1$ in the cylindrical coordinate system, we obtain:

$$P_{zs}^{(E)}(r,\varphi,\omega) = \left(\frac{\omega\mu_0}{2\pi}\right)^2 |P(\omega)|^2 \left|\tilde{\Phi}_s(\omega)\right|^2 F(r,\varphi); \quad (44)$$
$$\tilde{\Phi}_s(\omega) = (1 - i\omega\tau)\exp(i\omega\tau) - 1.$$

In formula (44) we identify:

$$F(r,\varphi) = 2N_0 d_0 \int_0^{r_0} r' dr' \left(1 - \frac{r'^2}{r_0^2}\right) \times \int_0^{2\pi} \frac{d\varphi'}{r^2 + r'^2 - 2r'r\cos(\varphi - \varphi')}. \quad (45)$$

We calculate the $\tilde{D}_r(\mathbf{r},\mathbf{r}',\omega)$ value using formula (34) in order to determine the spectrum of the electromagnetic radiation, which is scattered because an electromagnetic wave is incident on random discharges in the troposphere. The scattered radiation is generated by the discharge current induced by an incident wave. Using the fact that the induced current depends on coordinates and time (24), from (34) and (35) we obtain:

$$D_r(\mathbf{r},\mathbf{r}',t) = \mathrm{Re}\left[\int_{-l/2}^{l/2} I(\mathbf{r},\xi,t + n_z\xi/c)d\xi\right]$$
$$\approx 2Cl^3 E_0(\mathbf{r})\,\mathrm{Im}\left[\Phi_r(t,n_z)\exp(-i\omega_0 t)\right]; \quad (46)$$
$$\tilde{D}(\mathbf{r},\mathbf{r}',\omega) = \int_{-\infty}^{\infty} \frac{d\omega}{2\pi} D_r(\mathbf{r},\mathbf{r}',t)\exp(-i\omega t).$$

In equality (46) we identify:

$$\Phi_r(t,n_z) = \frac{\omega_0 \cos\left(\frac{k_0 n_z l}{2}\right)}{(ql)\left[(ql)^2 - (k_0 n_z l)^2\right]} \times \left[\tan\left(\frac{ql}{2}\right) - \frac{q}{k_0 n_z}\tan\left(\frac{k_0 n_z l}{2}\right)\right]. \quad (47)$$

Substituting (46) and (47) in (32), we obtain the following expression for the scattered radiation narrowband spectrum:

$$P_z^{(E)}(\mathbf{r},\omega) = \left(\frac{\omega\mu_0}{2\pi}\right)^2 P_0^2 \int_V f^2(\mathbf{r}')N(\mathbf{r}')\frac{\left(1 - n_z^2\right)^2}{|\mathbf{r} - \mathbf{r}'|^2} \times \left|\tilde{\Phi}_r(\omega - \omega_0, n_z)\right|^2 \mathrm{d}\,\mathbf{r}'; \quad (48)$$
$$P_0 = Cl^3 E_m; \quad \tilde{\Phi}_r(\omega,n_z) = \int_{-\infty}^{\infty} \Phi_r(t,n_z)\exp(i\omega t)dt.$$

In relationships (48) it is accepted that the spatial distribution of the incident electric field amplitude $E_0(\mathbf{r})$ is defined by formula $E_0(\mathbf{r}) = E_m f(\mathbf{r})$, where $E_m$ is the field value at the center of the region occupied by discharges and $f(\mathbf{r})$ is the dimensionless function. We assume that the incident wave field amplitude varies insignificantly $f(\mathbf{r}) \approx 1$ in this region $r \le r_0$. Selecting the $N(\mathbf{r})$ distribution in form (38) and taking into account the fact that $n_z \sim h/r \ll 1$ at large distances, from (48) we obtain the following relationship in the cylindrical coordinate system on the $x$ axis (at $\varphi = 0$):

$$P_{zr}^{(E)}(r,\varphi,\omega) = \left(\frac{\omega\mu_0}{2\pi}\right)^2 P_0^2 \left|\tilde{\Phi}_r(\omega - \omega_0)\right|^2 F(r,\varphi). \quad (49)$$

In equality (49) we identify:

$$\tilde{\Phi}_r(\omega) = \int_{-\infty}^{\infty} \Phi_r(t)\exp(i\omega t)dt;$$
$$\Phi_r(t) = \frac{\omega_0}{(ql)^3}\left[\tan\left(\frac{ql}{2}\right) - \frac{ql}{2}\right]. \quad (50)$$

We consider a change in the power spectrum along the $x$ axis. Assuming that $\varphi = 0$ in (45) and integrating over $\varphi'$ and $r'$, we obtain the following expression for $r > r_0$:

$$F(r) = 2\pi N_0 d_0 \left[1 + \left(\frac{r^2}{r_0^2} - 1\right)\ln\left(1 - \frac{r_0^2}{r^2}\right)\right]. \quad (51)$$

Substituting (51) in formulas (39) and (41), we obtain:

$$P_{zs}^{(E)}(r,\varphi = 0,\omega) = \left(\frac{\omega\mu_0}{2\pi}\right)^2 |P(\omega)|^2 \left|\tilde{\Phi}_s(\omega)\right|^2 F(r);$$
$$P_{zr}^{(E)}(r,\varphi = 0,\omega) = \left(\frac{\omega\mu_0}{2\pi}\right)^2 P_0^2 \left|\tilde{\Phi}_r(\omega - \omega_0)\right|^2 F(r). \quad (52)$$

## REFERENCES


Creagh, D.C., Fletcher, N.H., and Somerville, J.M., The decay of a spark channel which has ceased to carry current, *Proc. Phys. Soc.*, 1963, vol. 81, pp. 480–489.

Fukumoto, Y., Hayakawa, M., and Yasuda, H., Investigation of over-horizon VHF radio signals associated with earthquakes, *Nat. Hazards Earth Syst. Sci.*, 2001, vol. 1, pp. 107–112.

Gokhberg, M.B., Morgunov, V.A., and Pokhotelov, O.A., *Earthquake Prediction: Seismo–Electromagnetic Phenomena*, Gordon and Breach, 1995.

Hata, M., Tian, X., and Takumi, I., ELF horizontal flux precursor of Moderate Yamashi-96 earthquake, *J. Atmos. Electr.*, 1996, vol. 16, no. 3, pp. 199–220.

Hata, M., Takumi, I. and Yabashu, S., A model of earthquake seen by electromagnetic observation—gaseous emission from the Earth as main source of pre-seismic electromagnetic precursor and trigger of followed earthquake, *Ann. Geophys.*, 1998, vol. 16 (suppl.), C1188.

Hayakawa, M., *Electromagnetic Phenomena Associated with Earthquakes*, Trivandrum, India: Transworld Research Network, 2009.

Iudin, D.I. and Trakhtengerts, V.Yu., Fractal structure of the nonlinear dynamics of electric charge in a thundercloud, *Radiophys. Quantum Electron.*, 2001, vol. 44, nos. 5–6, pp. 386–402.

Moriya, T., Mogi, T., and Takada, M., Anomalous preseismic transmission of VHF-band radio waves resulting from large earthquakes, and its statistical relationship to magnitude of impending earthquakes, *Geophys. J. Int.*, 2010, vol. 180, pp. 858–870.

Nagao, T., Enomoto, Y., Fujinawa, Y., et al., Electromagnetic anomalies associated with 1995 Kobe earthquake, *J. Geodyn.*, 2002, vol. 33, pp. 401–411.

Nomikos, K., Vallianatos, F., Kaliakatsos, I., Saderis, E., and Bakatsakis, M., The latest aspects of telluric and electromagnetic variations associated with shallow and intermediate depth earthquakes in the South Aegean, *Ann. Geophys.*, 1997, vol. 50, no. 2, pp. 361–374.

Orville, R.E., Temperature and electron density in long air sparks, *J. Appl. Phys.*, 1967, vol. 38, pp. 895–901.

Papadopoulos, G.A., Luminous and fiery phenomena associated with earthquakes in East Mediterranean, in *Atmospheric and Ionospheric EM Phenomena Associated with EQ*, Hayakawa, M., Ed., Tokyo: Terrapub, 1999, pp. 559–575.

Pilipenko, V., Shalimov, S., Uyeda, S., et al., Possible mechanism of the over-horizon reception of fm radio waves during earthquake preparation period, *Proc. Jpn. Acad., Ser. B*, 2001, vol. 77, pp. 125–130.

Proctor, D.E., Uytenbogaardt, R., and Meredith, B.M., VHF radio pictures of lightning flashes to ground, *J. Geophys. Res.*, 1988, vol. 93, no. D10, pp. 12683–12727.

Rakov, V.A. and Uman, M.A., *Lightning: Physics and Effects*. Cambridge, U.K., New York: Cambridge University Press, 2003.

Ruzhin, Y. and Nomicos, C., Radio VHF precursors of earthquakes, *Nat. Hazards*, 2006, vol. 40, pp. 573–583.

Sadiku, M., *Elements of Electromagnetics*, New York: Oxford University Press, 2007.

Sakai, K., Takano, T., and Shimakura, S., Observation system for anomalous propagation of FM radio broadcasting wave related to earthquakes and preliminary result, *J. Atmos. Electr.*, 2001, vol. 21, pp. 71–78.

Sorokin, V. and Hayakawa, M., Generation of seismic-related DC electric fields and lithosphere–atmosphere–ionosphere coupling, *Mod. Appl. Sci.*, 2013, vol. 7, no. 6, pp. 1–25.

Sorokin, V.M., Ruzhin, Y.Y., Yaschenko, A.K., and Hayakawa, M., Generation of VHF radio emissions by electric discharges in the lower atmosphere over a seismic region, *J. Atmos. Sol.-Terr. Phys.*, 2011, vol. 73, pp. 664–670.

Sorokin, V.M., Ruzhin, Y.Y., Yaschenko, A.K., and Hayakawa, M., Seismic-related electric discharges in the lower atmosphere, in *The Frontier of Earthquake Prediction Studies*, Hayakawa, M., Ed., Tokyo: Nihon-Senmontosho-Shuppan, 2012a, pp. 592–611.

Sorokin, V., Ruzhin, Y., Kuznetsov, V., and Yaschenko, A., Model of electric discharge formation in the lower atmosphere over a seismic region, *Geomatics Nat. Hazards Risk*, 2012b, vol. 3, pp. 225–238.

Sorokin, V.M., Yaschenko, A.K., and Hayakawa, M., Scattering of VHF transmitter signals by seismic-related electric discharges in the troposphere, *J. Atmos. Sol.-Terr. Phys.*, 2014, vol. 109, pp. 15–21.

Sorokin, V.M., Chmyrev, V.M., and Hayakawa, M., *Electrodynamic Coupling of Lithosphere–Atmosphere–Ionosphere of the Earth*, New York: Nova Science, 2015.

Uman, M.A. and Voshall, R.E., Time interval between lightning strokes and the initiation of dart leaders, *J. Geophys. Res.*, 1968, vol. 73, no. 2, pp. 497–506.

Vallianatos, F. and Nomikos, K., Seismogenic radioemissions as earthquake precursors in Greece, *Phys. Chem. Earth*, 1998, vol. 23, pp. 953–957.

Van Bladel, J., *Electromagnetic Fields*, Hoboken, N.J.: Wiley, 2007.

Varotsos, P. and Alexopoulos, K., Physical properties of the variations of the electric field of the earth preceding earthquakes. II. Determination of epicenter and magnitude, *Tectonophysics*, 1984, vol. 110, pp. 99–125.

Voinov, V.V., Gufel'd, I.L., and Kruglikov, V.V., Effects in the ionosphere and atmosfere before the Spitak earthquake on December 7, 1988, *Izv. Akad. Nauk SSSR, Fiz. Zemli*, 1992, no. 3, pp. 96–102.

Voldman, S.H., *ESD: Physics and Devices*. Hoboken, N.J.: Wiley, 2004.

Warwick, J.W., Hayenga, C.O., and Brosnahan, J.W., Interferometric directions of lightning sources at 34 MHz, *J. Geophys. Res.*, 1979, vol. 84, no. C5, pp. 2457–2467.

Williams, E.R., Geotis, S.G., and Bhattacharya, A.B., A radar study of the plasma and geometry of lightning, *J. Atmos. Sci.*, 1989, vol. 46, pp. 1173–1185.

Yaglom, A.M., *Correlation Theory of Stationary and Related Random Functions*, New York: Springer, 1987.

Yamada, A., Sakai, K., Yaji, Y., et al., Observation of natural noise in VHF band which relates to earthquakes, in *Seismo Electromagnatics: Lithosphere–Atmosphere–Ionosphere Coupling*, Hayakawa, M. and Molchanov, O.A., Eds., Tokyo: Terrapub, 2002, pp. 255–257.

Yos, J.M., *Transport Properties of Nitrogen, Hydrogen, Oxygen, and Air to 30000 K*, Defense Technical Information Center, 1963.

Zhao, Y. and Qian, F., Earthquake lights: A very convincing evidence for energy transfer from earth to air, in *Abstracts of the International Workshop on Seismo Electromagnetics*, Tokyo, 1997, p. 242.

*Translated by Yu. Safronov*